EurJOC
European Journal of Organic Chemistry

Research Article
doi.org/10.1002/ejoc.202200649

Chemistry Europe
European Chemical Societies Publishing

www.eurjoc.org

Special Collection

Calix[4]arene-Based Sensitizers for Host-Guest Supramolecular Dyads for Solar Energy Conversion in Photoelectrochemical Cells.

Cristina Decavoli,[a] Chiara L. Boldrini,[a] Federica Faroldi,[b] Laura Baldini,*[b] Francesco Sansone,[b] Anna Ranaudo,[c] Claudio Greco,[c] Ugo Cosentino,*[c] Giorgio Moro,[d] Norberto Manfredi,*[a] and Alessandro Abbotto*[a]

Dedicated to Professor Cesare Gennari on the occasion of his 70th birthday

The photogeneration of electricity and solar fuels by solar irradiation in photoelectrochemical cells is one of the sectors with the highest growth potential in the decarbonised society. However, the use of different components, in particular photosensitizers and catalysts, can present problems of charge transfer efficiency at the interface, leading to lower final efficiencies. In this work we present novel integrated photosensitizer-catalyst dyads based on robust and, at the same time, flexible host-guest non-covalent interactions through the use of calix[4]arene cavities. Current photogeneration in photoelectrochemical cells showed twice greater efficiency in the integrated calixarene-based host-guest dyads compared to the traditional architecture based on the separate photosensitizer-catalyst pair. Molecular dynamics studies have shown that the enhanced performance originates from an optimization of the distances between the centres of the photosensitizer, catalyst and semiconductor involved in the charge transfer processes, thus allowing a higher final efficiency of the charge photogeneration process.

Introduction

The definitive affirmation of an energy policy not dependent on fossil fuels is one of the most important goals of the next decades.[1] The impact of human activities on the environment and the social disparity generated by the distribution of such resources are direct consequences of the exploitation of non-renewable sources.[2] Moreover, the need for hydrocarbons as a feedstock for carbon-based chemicals claims a reduction of the consumption of these precious resources in energy production to keep their price acceptable.[3] In this scenario, direct light-driven production of electricity and fuels represents an important alternative. Photovoltaics and photoelectrochemical water splitting are emerging technologies able to reduce the share of fossil fuels in primary energy consumption.[2c,4] Dye-sensitized solar technologies (Dye-Sensitized Solar Cells, DSSCs, and Dye-Sensitized Photoelectrochemical Cells, DS-PECs) hold a great potential and flexibility for solar-induced generation of electricity and fuels thanks to their multi-component architecture.[5] The possibility to tune up single properties, and thus the final device response, just varying the nature and the structure of the single components, for example the photosensitizers, keeping their main device structure, opens a wide range of choices and performances in terms of final application.[6]

A DS-PEC is a photoelectrocatalytic device where water splitting could take place performing the water oxidation at the (photo)anode and the proton reduction at the (photo)cathode (Figure 1). Compared to a PEC, where the water splitting process at each electrode is covered by one component, e.g. a semiconductor such as TiO_2,[7] in a DS-PEC, light-harvesting and catalysed water splitting are separated and accomplished by different components, which gives the chance to separately optimize their activity. In such devices, light-harvesting and

[a] Dr. C. Decavoli, Dr. C. L. Boldrini, Dr. N. Manfredi, Prof. A. Abbotto
Department of Materials Science and Milano-Bicocca Solar Energy Research Center – MIB-Solar
University of Milano-Bicocca
Via Cozzi 55, 20125 Milano, Italy
E-mail: norberto.manfredi@unimib.it
alessandro.abbotto@unimib.it
[b] Dr. F. Faroldi, Prof. L. Baldini, Prof. F. Sansone
Dipartimento di Scienze Chimiche,
della Vita e della Sostenibilità Ambientale
University of Parma
Parco Area delle Scienze 17/A, 43124, Parma, Italy
E-mail: laura.baldini@unipr.it
[c] Dr. A. Ranaudo, Prof. C. Greco, Prof. U. Cosentino
Department of Earth and Environmental Sciences,
University of Milano-Bicocca,
Piazza della Scienza 1, 20126 Milano, Italy
E-mail: ugo.cosentino@unimib.it
[d] Prof. G. Moro
Department of Biotechnology and Biosciences,
University of Milano-Bicocca,
Piazza della Scienza 2, 20126 Milano, Italy

Supporting information for this article is available on the WWW under https://doi.org/10.1002/ejoc.202200649

Part of the "Cesare Gennari's 70th Birthday" Special Collection.

Research Article
doi.org/10.1002/ejoc.202200649

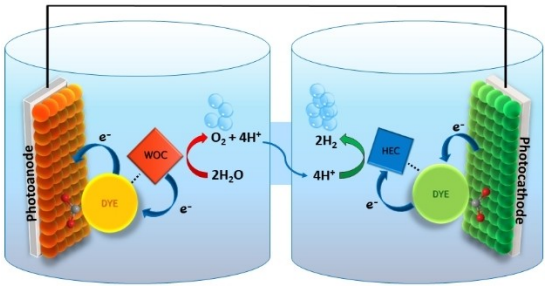

Figure 1. Schematic representation of a DS-PEC.

charge injection at the photoactive electrode is performed by a photosensitizer.[5e] The generated charges (electrons in a photoanode or holes in a photocathode) are then transferred from the dye to a n- or p-type semiconductor, respectively.[8] Consequently, a radical cation or anion of the dye is obtained. The neutral state of the sensitiser is then regenerated by the extraction of electrons from a water oxidation catalyst (WOC) for the photoanode and holes from a hydrogen evolution catalyst (HEC) for the photocathode, affording water oxidation and reduction at the water-catalyst interface. A careful control and optimization of all the charge transfer processes at the water-catalyst-dye interfaces, namely from water to the catalyst and from the catalyst to the dye, is thus of principal importance to optimize the efficiency of the whole process.

The use of organic sensitizers in DSSCs is well documented in the literature of the last two decades and a plethora of molecules have been reported with successful results.[9] In the case of DS-PECs, the almost new-born research field is still relatively at its infancy, with particular reference to the use of metal-free dyes. In fact, most of the sensitizers used in DS-PECs are Ru-based organometallic compounds and metal-free molecules represent just a minority.[5e,10] Furthermore, the use of supramolecular assemblies in this field is almost absent, especially for water oxidation application.

Two methods are commonly used in DS-PEC to organize the multicomponent device structure. The first one is the covalent grafting of both the dye and the catalyst, separately, onto the surface of the semiconductor.[11] The second approach is the deposition of an integrated dye-catalyst dyad, where the catalyst is directly linked through covalent bonds to the sensitizer, in turn grafted onto the semiconductor surface.[12] In the former case, the main drawback is related to the competitive effect of the back-electron transfer from the semiconductor to the sensitizer with the hole scavenging by catalyst. Moreover, the poor intermolecular charge transport between the dyes and the catalysts adsorbed onto the semiconductor hinders the multiple oxidative process required for water oxidation. In contrast, in the case of a dye-catalyst dyad, the electron transfer process is favoured since the catalyst is directly bonded to the dye. This aspect is also associated to faster electron injection from the dyad to the semiconductor, thus limiting detrimental back-electron transfer from the semiconductor to the oxidized sensitizer. A serous drawback of this approach, however, is the need to previously build the dye-catalyst dyad and, only subsequently, anchor the dyad to the semiconductor. This step may represent important issues due to the poor stability of the dyad. Therefore, a supramolecular approach where the dye-catalyst interaction is promoted by non-covalent bonds may represent an attractive route to circumvent this problem.

Recently, Sun and co-workers have described the use of flexible host-guest supramolecular assembly formed by insertion of a water oxidation catalyst (WOC) into the cavity of a β-cyclodextrin (β-CD)-modified ruthenium based sensitizers.[13] β-Cyclodextrin possesses a molecular cavity capable of hosting different small guests, with a selectivity regulated by the cavity size and, together with calixarenes and cucurbiturils, is one of the most investigated host structures in chemistry.

Calix[4]arenes are synthetic phenol-formaldehyde macrocycles widely exploited not only as hosts[14] but also as scaffolds for the construction of functional molecular[15] or supramolecular complex structures.[16] Both their rims can be easily functionalized and their conformation can be locked in the cone structure by the introduction of alkyl chains bulkier than ethyl. The macrocyclic cavity of calix[4]arenes is aromatic and is therefore capable of hosting guest molecules via π-π and CH-π interactions,[17] with high efficiency also in water.[18] The use of calix[4]arene for photovoltaics and water splitting is still scantly reported in the literature, and only few studies have been published.[19]

In this work, we report the first example of calixarene-based dye-catalyst supramolecular dyads for water splitting in DS-PECs.[20] In particular, we combine the valuable host-guest properties of calix[4]arenes with easy-to-synthesize metal-free organic dye-sensitizers to prepare supramolecular assemblies with commonly used WOC (Figure 2).

We show that the ability of the calix[4]arene scaffold to properly host the WOC results in a more efficient interaction (charge transfer) between the catalyst WOC and the photosensitizer, in turn affording more efficient photoinduced water splitting. Moreover, our study also highlights different mobility of the anchored dyes on the TiO_2 surface that could affect the electron-transfer process to the surface.

Results and Discussion

Design and Synthesis

p-*tert*-Butylcalix[4]arene was chosen as a host moiety because of its efficient binding properties towards aromatic units. In particular, p-*tert*-butylcalix[4]arene is well known to form an inclusion complex with toluene both at the solid state[21] and when grafted on a solid support, in the latter case adsorbing toluene from a water solution.[22] The guest unit enters the calixarene cavity by its methyl group and the complex is stabilized by multiple CH-π interactions.[23]

The supramolecular calixarene-based dye-catalyst dyad has therefore been designed upon this favourable interaction: we assumed that the 4-picoline ligand of **[Ru(bda)(pic)$_2$]**, (bda =

Research Article
doi.org/10.1002/ejoc.202200649

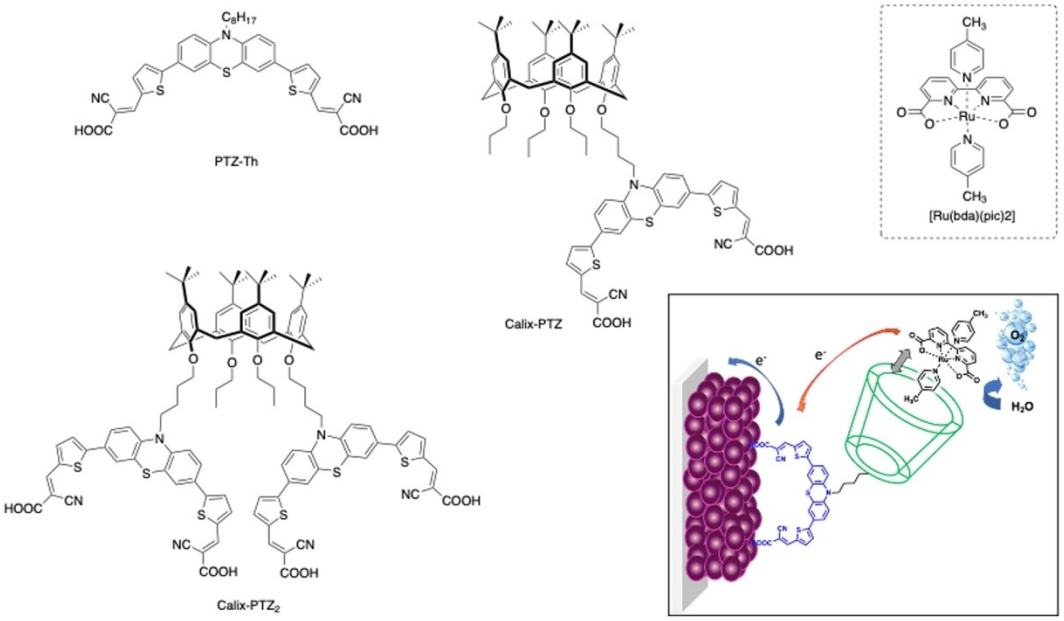

Figure 2. Structures investigated and aim of this work.

2,2′-bipyridine-6,6′-dicarboxylate, pic = 4-picoline), a commonly used Ru-based WOC for water splitting,[24] might be easily complexed by the cavity of a p-*tert*-butylcalix[4]arene derivative functionalized at the lower rim with a phenothiazine-based dye (**PTZ-Th**), a photosensitizer previously investigated by us in photoelectrochemical water splitting.[25] Two calixarene-dye precursors have been investigated for the host-guest supramolecular interaction with WOC: **Calix-PTZ**, where the calix[4]arene moiety has been linked to one molecule of the dye, and **Calix-PTZ$_2$**, where two **PTZ-Th** units have been covalently linked (Figure 2). In both cases, the dyes have been connected to the calixarene through a *n*-butyl spacer, to provide the system with a good degree of flexibility, and the remaining positions of the lower rim have been functionalized with *n*-propyl chains to fix the calixarene scaffold in the cone structure.

Our aim was to investigate the efficacy of supramolecular host-guest interactions in water splitting as a function of the number of units of sensitizer. The water splitting analysis will then be compared to that of a DS-PEC where the interaction of the simple dye **PTZ-Th** and the catalyst **[Ru(bda)(pic)$_2$]** is not mediated by the calixarene host.

The calix[4]arene derivatives, the simple sensitizer **PTZ-Th**, and the ruthenium catalyst **[Ru(bda)(pic)$_2$]** were synthesized according to literature.[24a,25a] The synthetic procedure for the preparation of the calix[4]arene precursors **2** and **4** is depicted in Scheme 1. 5,11,17,23-Tetra-*tert*-butyl-25,26,27-tripropoxycalix[4]arene (**1**) and 5,11,17,23-tetra-*tert*-butyl-25,27-dipropoxycalix[4]arene (**3**) were synthesized according to literature procedures.[26] The alkylation reactions to precursors **2** and **4** were performed under inert atmosphere in DMF using 1,4-diiodobutane in presence of NaH as a base. The reactions gave

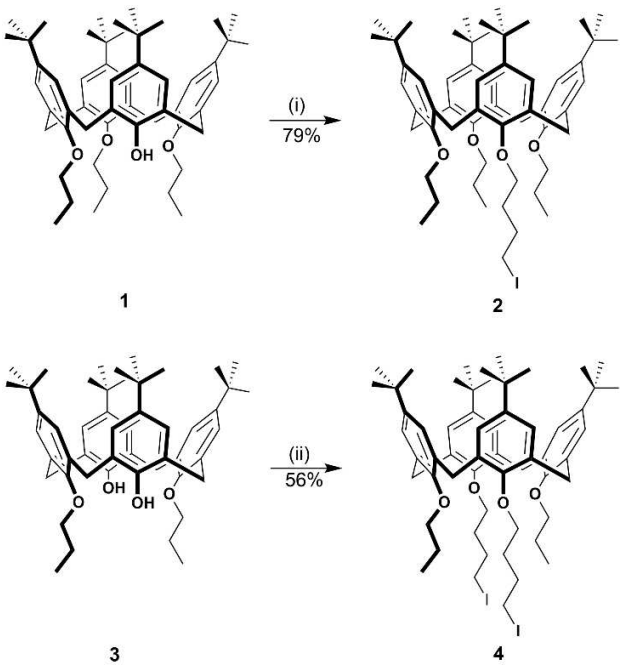

Scheme 1. Synthesis of calix[4]arene intermediates **2** and **4**. Reagents and conditions: (i) 1,4-diiodobutane, NaH, anhydrous DMF, rt, 5 h; (ii) 1,4-diiodobutane, NaH, anhydrous DMF, rt, 3 h.

the products in good yield after neutralization with 0.1 N HCl and column chromatography.

The synthesis of the calix[4]arene-based supramolecular dye-host precursors, **Calix-PTZ** and **Calix-PTZ$_2$**, is depicted in Scheme 2. A Suzuki cross-coupling reaction, in presence of $Pd(dppf)Cl_2$ and K_2CO_3 in DME/MeOH, under microwave irradiation, was carried out between 3,7-dibromo-10*H*-

Research Article
doi.org/10.1002/ejoc.202200649

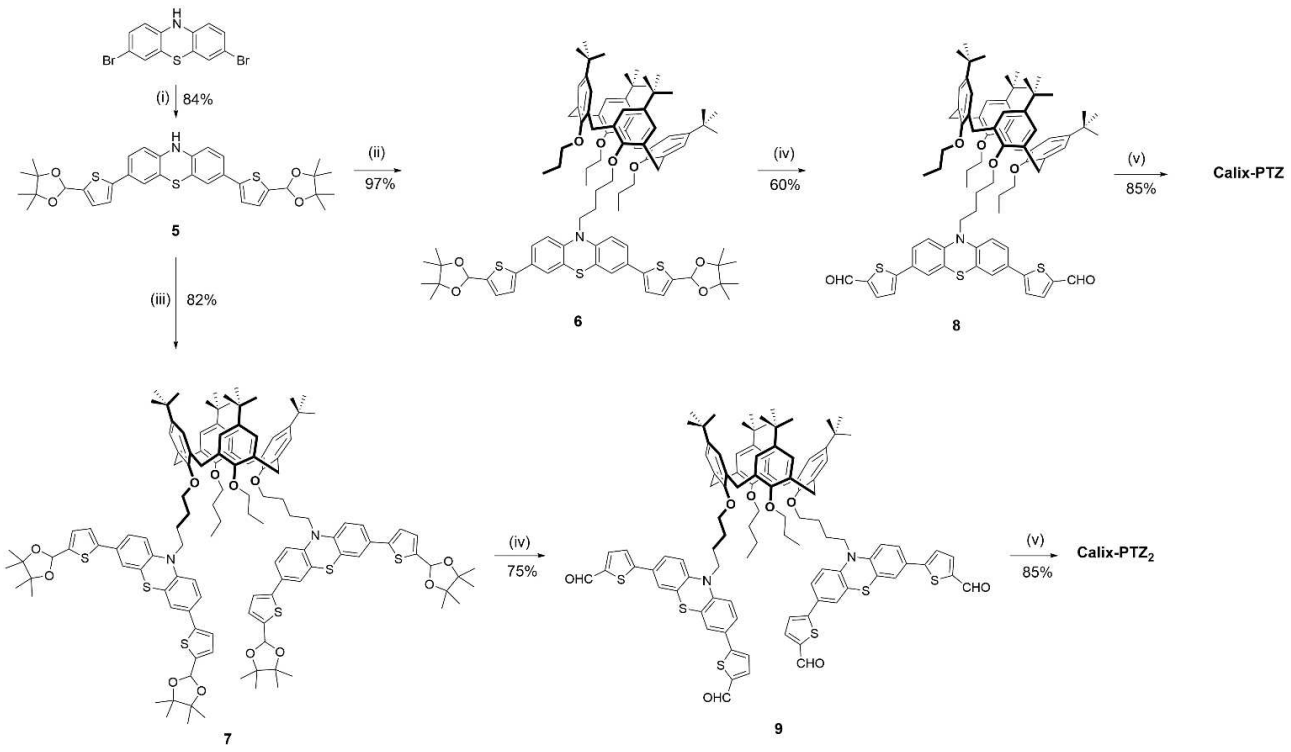

Scheme 2. Synthesis of **Calix-PTZ** and **Calix-PTZ$_2$**. Reagents and conditions: i) 4,4,5,5-Tetramethyl-2-[5-(4,4,5,5-tetramethyl-1,3-dioxolan-2-yl)- thiophen-2-yl]-1,3,2-dioxaborolane, Pd(dppf)Cl_2, K_2CO_3, DME-MeOH 1:1 v/v, μw 75 W, 90 min, 90 °C; ii) **2**, NaH, DMF, rt, 1 days; iii) **4**, NaH, anhydrous DMF, rt, 3 days; iv) THF-10% HCl_{aq} 1:2 v/v, 50 °C, 3 days; v) cyanoacetic acid, piperidine, $CHCl_3$, reflux, 4 days.

phenothiazine[25b] and 5-formylthienyl-2-boronic acid, protected as pinacol acetal to avoid possible side-reactions during the calixarene derivatization step.[27] The cross-coupling afforded the intermediate **5** in good yield after proper work-up and column chromatography. Subsequent nucleophilic substitution under inert atmosphere in DMF for 3 days, in presence of NaH as a base, with the proper iodobutyl calix[4]arene derivative (**2** for the **Calix-PTZ** precursor, and **4** for the **Calix-PTZ$_2$** precursor) afforded intermediates **6** and **7**. The two products were purified and submitted to deprotection with 10% HCl_{aq}/THF 1:2 v/v at 50 °C to regenerate the free formyl functionalities in **8** and **9**. Final Knoevenagel-type condensation with cyanoacetic acid in chloroform at reflux afforded the desired calixarene-dye precursors **Calix-PTZ** and **Calix-PTZ$_2$**.

The calixarene-based dyes **Calix-PTZ** and **Calix-PTZ$_2$** have been optically and electrochemically characterised both in solution and chemisorbed on a TiO_2 film. The UV-Vis spectra of the sensitizers compared with the reference dye **PTZ-Th** are depicted in Figure 3 and the main relevant parameters are collected in Table 1. The optical response of the calixarene-dyes **Calix-PTZ** and **Calix-PTZ$_2$** is similar to that of the reference dye **PTZ-Th**, as expected on the basis of the fact that the calixarene moiety does not perturb the π-conjugated framework of the donor-acceptor fragment, being linked to the chromophore units by saturated alkyl chains. The three dyes exhibited, in the visible region, the same 2-band structure, ascribed to local π-π* absorption in the 350–400 nm range and to the ICT transition in the 400–600 nm range, respectively. The absorption spectra in the UV region were not investigated since they are not relevant of the specific application. In fact, when sensitizers are used in a DS-PEC, the portion of the UV spectrum overlaps with that of the semiconductor (and, accordingly, irradiation light is filtered in the UV region). The intensity of the absorption mainly follows the trend given by the number of chromophore units per mole

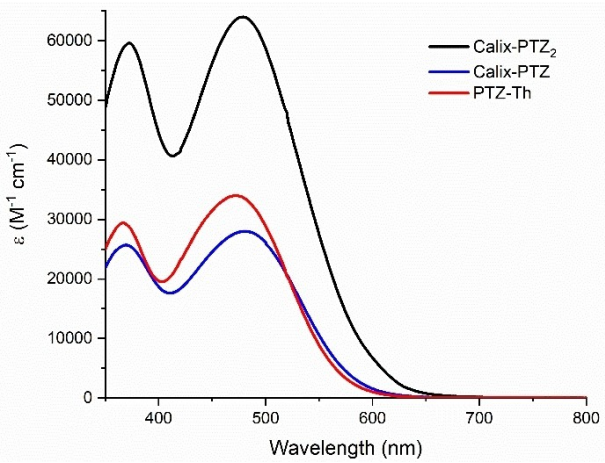

Figure 3. Absorption spectra of the sensitizers **Calix-PTZ** and **Calix-PTZ$_2$** in DMSO solution (10^{-5} M) compared to the reference dye **PTZ-Th**.

Research Article
doi.org/10.1002/ejoc.202200649

Table 1. Optical and electrochemical parameters of investigated sensitizers in solution and on transparent TiO_2 film (in brackets).

Sample	λ_{max} [b,c] [nm]	λ_{onset} [b,c] [nm]	ε [$M^{-1}cm^{-1}$]	V_{ox} [d,e] [V vs NHE] ±10 mV	HOMO [d,e,f] [eV] ±0.05 eV	E_{gap} opt[b,e] [eV]	LUMO [d,e,g] [eV] ±0.05 eV
PTZ-Th[a]	470	592	34000	0.88	−5.48	1.90	−3.58
	(463)	(657)	±1000	(0.84)	(−5.44)	(1.70)	(−3.74)
Calix-PTZ	481	594	28000	1.06	−5.66	1.89	−3.77
	(457)	(618)	±1000	(0.93)	(−5.53)	(1.84)	(−3.69)
Calix-PTZ$_2$	478	624	64000	1.02	−5.62	1.83	−3.79
	(462)	(628)	±1000	(0.93)	(−5.53)	(1.74)	(−3.79)

[a] Value from ref. 6. [b] Dye solution 10^{-5} M in DMSO. [c] 1-μm-thick transparent TiO_2 photoanode films in brackets. [d] 10^{-4} M dye solution in $TBABF_4$ 0.1 M DMF. [e] 3.5-μm transparent TiO_2 photoanode films in 0.5 M KNO_3 PBS pH 6.5 in brackets. [f] Molecular orbital energy vs vacuum = −4.60 eV − NHE.[31] [g] LUMO energy = HOMO energy + E_{gap}.

of compound. Accordingly, **PTZ-Th** and **Calix-PTZ** have similar molar absorptivities whereas that of **Calix-PTZ$_2$** is almost twice.

The absolute value is in agreement with previous analogous systems reported in the literature.[28] The absorption spectra on 1-μm-thick TiO_2 films presented a shape similar to those in solution (Figure S1, see Supporting Information). The absorption maxima are blue-shifted by ca. 30 nm, in agreement with the formation of covalent bonds involving the carboxylic acid groups and the titanium dioxide, thus reducing the electron-withdrawing strength of the acceptor groups in the dye. Optical bandgaps have been calculated by means of the Tauc plots.[29] Unfortunately, it was not possible to estimate the amount of sensitizer chemisorbed on the films by typical desorption in basic media (hydrolysis of the bond between the dye and TiO_2) due to the high stability of the dye anchoring under these conditions, which, on the other hand, is encouraging for long-term stability applications.

The oxidation potentials of **Calix-PTZ** and **Calix-PTZ$_2$** were determined using cyclic voltammetry (CV) and differential pulse voltammetry (DPV) when dissolved in 0.1 M $TBABF_4$ in DMF solution and when chemisorbed onto TiO_2 films using an aqueous buffer. The corresponding results are depicted in Figure S2-S4 (see Supporting Information) and listed in Table 1. The oxidation potential of **PTZ-Th** has been previously determined and collected in Table 1 as a reference. All of the compounds showed irreversible oxidation peaks in the CV profile in solution. For this reason, DPV was preferred. The first oxidation peak was attributed to the oxidation of the dye. The oxidation potentials, which dictate the HOMO energy, are positive enough to drive water oxidation, whereas the LUMO level, estimated from the HOMO energy and the optical bandgap, is high enough to inject excited electrons in the conduction band (CB) of TiO_2 (−4 eV).[30]

To further investigate the behavior of the new sensitizers in the operative environment, CV and DPV measurements of the dye-sensitized photoanodes were also performed using a 3-electrode electrochemical cell in phosphate buffered saline (PBS) solution + KNO_3 0.5 M at pH = 6.5 (Figure S4 and Figure S5, see Supporting Information). The sensitized TiO_2 photoanode acted as the working electrode, a Pt wire as the counter electrode, and Ag/AgCl (KCl 3 M) as a reference electrode. All the measurements showed an irreversible oxidation peak between +0.9 and +1.1 V *vs* NHE. The recorded oxidation potential was in the order **Calix-PTZ$_2$** > **Calix-PTZ** > **PTZ-Th**. **PTZ-Th** presented the highest current density, while **Calix-PTZ$_2$** produced a current density higher than **Calix-PTZ**.

The electrochemical characterization of the photoanodes was also performed with the investigated WOC dissolved in the electrolyte medium (Figure 4). In this case, the WOC was dissolved in CF_3CH_2OH and then added to the PBS solution in the electrochemical cell (1×10^{-3} M).[13] In all CV profiles, the current density in presence of the WOC increased with respect to the measurement without the catalyst, especially for the peak at +1.2 V *vs* NHE, which corresponds to the beginning of the catalytic wave for water oxidation.[32] A reversible oxidation peak attributed to **[Ru(bda)(pic)$_2$]** was clearly present in all CV profiles. However, in the **Calix-PTZ** voltammogram, this peak was broader and shifted (+0.81 V and +0.44 V vs NHE for oxidation and reduction potentials, respectively) compared to the other investigated dyes (+0.71 V and +0.63 V *vs* NHE for oxidation and reduction potentials, respectively). Indeed, the oxidation peak at +0.81 V *vs* NHE indicated the presence of the Ru^{III}/Ru^{IV} couple, that is mandatory to perform water

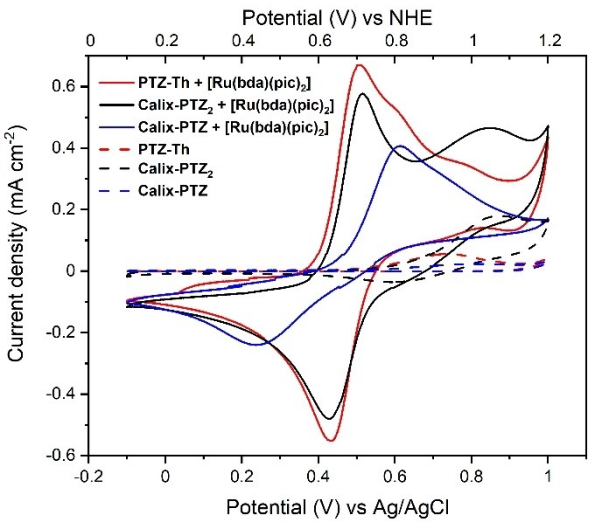

Figure 4. CV of the dye-sensitized photoanodes in presence or in absence of **[Ru(bda)(pic)$_2$]**. Conditions: spectra without the catalysts were recorded in PBS solution + KNO_3 0.5 M at pH 6.5; spectra with the WOC were recorded in PBS solution + KNO_3 0.5 M at pH 6.5 + 5% CF_3CH_2OH (v/v). Counter electrode = Pt wire, reference electrode = Ag/AgCl KCl 3 M, scan rate 50 mV s^{-1}.

Research Article
doi.org/10.1002/ejoc.202200649

oxidation.[32] Interestingly, Figure 4 shows a peculiar feature of **Calix-PTZ** in presence of WOC, compared to the other two investigated species. Indeed, **Calix-PTZ** shows a single broad oxidation wave centred at ~ +0.8 V vs NHE, which can be attributed to a new species where the WOC interacts with the calix[4]arene cavity forming a single integrated photoactive species. In contrast, **Calix-PTZ$_2$** and **PTZ-Th** CV profiles show distinct oxidation peaks attributed, in the former case, to the two distinct original species (that is, the sensitizer and the catalyst), and in the latter one to the two original components as well as the new interactive species (for a total of 3 oxidation waves).

In all cases, the onset of the catalytic current was less positive than the oxidation potential of the dye on film, thus indicating that the photocatalytic water oxidation is thermodynamically favoured in these systems.[13]

The photosystems were studied in DS-PECs with the same set-up used for the electrochemical investigations. Linear sweep voltammetry (LSV) measurements were performed, both under illumination (200 W Xe lamp, $400 < \lambda < 800$ nm) and in the dark, in presence of the WOC (Figure S6, see Supporting Information). The different response of each photosystem in the dark and under illumination confirmed their photoactive behavior. In particular, photocurrents generated by **Calix-PTZ** and **PTZ-Th** were higher under irradiation and similar to each other, at oxidative potentials higher than +0.3 V *vs* NHE (~20 vs 25 μA cm^{-2}). In contrast, the current density of illuminated **Calix-PTZ$_2$** was almost comparable to that generated in the dark. A bias of +0.4 V vs NHE was thus adopted to maximize the photocurrents in the subsequent chronoamperometric (CA) characterization.

CA experiments were performed with the same set-up as for LSV, with 1 one-minute-chopped illumination cycles followed by 5 min of continuous irradiation (Figure 5). At every light-shutter opening, a photocurrent spike was observed. This is consistent with the initial fast charge separation due to the efficient electron injection from the excited dye to the CB of TiO_2, followed by extensive hole-electron recombination.[13] The surface recombination is likely the result of the slow catalytic kinetics of the catalyst, which is unable to completely consume the photogenerated holes.[13,33]

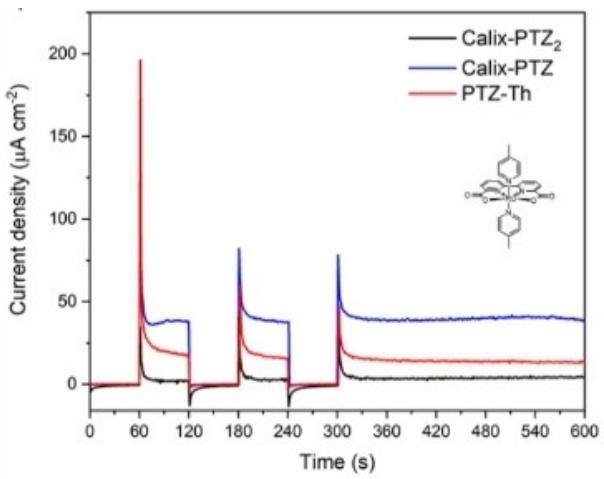

Figure 5. CA measurements of the investigated dyes with [Ru(bda)(pic)$_2$] in PBS electrolyte solution and 0.5 M KNO_3 + 5% CF_3CH_2OH (v/v) at pH 6.5 under illumination (200 W Xe lamp; $400 < \lambda < 800$ nm). CE = Pt wire, RE = Ag/AgCl KCl 3 M, applied bias +0.4 V vs NHE.

CA measurements revealed the following order in the photocurrent density generation: **Calix-PTZ** (~40 μA cm^{-2}) > **PTZ-Th** (~20 μA cm^{-2}) > **Calix-PTZ$_2$** (~0 μA cm^{-2}). The latter showed an almost negligible photoresponse. Notably, **Calix-PTZ** showed excellent stability with time and no decrease in the photocurrent along all the experiment. A similar result was observed for **PTZ-Th**, where only a small photocurrent decrease (from 17 to 14 μA cm^{-2}) was recorded.

Remarkably, the presence of the calix[4]arene moiety in **Calix-PTZ** allowed a photocurrent response approximately twice as larger as that of the reference **PTZ-Th**. The optical investigation (Figure 3), where the absorption intensity of **Calix-PTZ** and **PTZ-Th** was similar, excluded that this result may arise from enhanced light harvesting. To further confirm this, the photoresponse of **Calix-PTZ$_2$**, for which the molar absorptivity was twice larger thanks to the presence of two chromophore units, was almost absent. Thus, we can conclude that clearly, the presence of the calix[4]arene host cavity is responsible for the enhanced photoactivity of **Calix-PTZ**, although the same beneficial role was not observed for **Calix-PTZ$_2$**, an aspect that will be rationalized in the Molecular Dynamics simulation section. As far as the catalyst-calixarene interaction is concerned, we argue that, as expected, some sort of beneficial host-guest interaction takes place between the dye and the catalyst WOC, most likely due to the 4-picoline ligand of **[Ru(bda)(pic)$_2$]** entering the calixarene cavity. Indeed, the *p-t*-butylcalix[4]arene could easily host small guest molecules. According to the literature, the four *t*-butyl groups interact with aromatic groups through a CH_{host}-π_{guest} interaction.[34] Small groups on the guest aromatic cycle could more easily enter the macrocycle and favour a better orientation of the phenyl ring in order to more fruitfully exploit the CH_{host}-π_{guest} interaction.[34–35] Accordingly, the methyl group of the 4-picoline ligand in **[Ru(bda)(pic)$_2$]** might better interact with the host cavity favouring the interaction with the macrocycle.

Molecular dynamics simulations

Molecular Dynamics (MD) studies were performed in order to gain deeper insights on the beneficial TiO_2-dye-catalyst intermolecular interactions occurring in **Calix-PTZ**, which in turn are responsible for the enhanced performance. At the same time, simulations can help in rationalizing the fact that **Calix-PTZ$_2$** generated a very low photocurrent, despite the presence of the calix[4]arene moiety and encouraging optical properties.

MD simulations involved the **PTZ-Th**, **Calix-PTZ**, and **Calix-PTZ$_2$** dyes anchored to the [101] anatase surface. For each dye, the simulation box included the dye, the TiO_2 slab (9.2 × 7.9 × 1.1 nm) and about 12000 water molecules (final dimensions: 9.2 × 7.9 × 6.0 nm). In the case of **Calix-PTZ** and **Calix-PTZ$_2$**, simulations have been performed including also the **[Ru-**

Research Article
doi.org/10.1002/ejoc.202200649

(bda)(pic)$_2$] catalyst, initially docked into the calix[4]arene cavity. In the case of **PTZ-Th**, the catalyst is believed to freely diffuse in solution and, for this reason, it was not included in the simulations.

Analysis of MD simulations shows that the catalyst persistently stays inside the calix[4]arene cavities of both **Calix-PTZ** and **Calix-PTZ$_2$** due to the intermolecular interactions between the 4-picoline moiety and the host (see movies in Supporting Information).

With the aim of identifying key reference points for the investigation of dyes mobility as one of the main determinants of the charge transfer processes, we calculated the HOMO and LUMO of a model of **PTZ-Th** where the alkyl chain has been replaced by a methyl group (**PTZ-Th-Me)** at the DFT level (Figure S7, see Supporting Information). The centre of the phenothiazine ring has been selected as representative of the HOMO position, while the centre of the thiophene rings has been selected as representative of the LUMO position.

T. J. Meyer et al. have thoroughly studied the influence of intra-assembly distance effects on intra-assembly and interfacial electron transfer dynamics in DS-PEC photoanode applications.[36] Accordingly, along the MD trajectories we sampled a series of geometrical parameters able to affect the efficiency of the electron transfer processes: a) the distances between the centre of the thiophene rings (Figure S7d, see Supporting Information) and the TiO_2 surface; b) the angles between the planes defined by the thiophene rings and the TiO_2 surface, assumed as representative of the orientation of the LUMO with respect to the TiO_2 surface; and c) the distance between the centre of the phenothiazine ring, (Figure S7d, see Supporting Information), and the ruthenium atom of the catalyst. Parameters a) and b) modulate the interfacial electron transfer from the photoexcited dye (that is, from the LUMO of the dye) to the semiconductor surface, whereas distance c) modulates the interfacial electron transfer from the catalyst to the HOMO of the dye.

The percentage frequency and the cumulative percentage frequency of the distances between the centre of the thiophene rings of the three dyes and the TiO_2 surface are shown in Figure 6. These data clearly show that **Calix-PTZ**, and to a lesser extent **PTZ-Th**, present distances shifted toward lower values than **Calix-PTZ$_2$**, suggesting a closer contact between the LUMO and the semiconductor surface.

Figure 7 shows, for the three dyes, the percentage frequency, and the cumulative percentage frequency, of the angles between the planes defined by the thiophene rings and the TiO_2 surface (angles reported within the 0–90° window). It can be noted that **Calix-PTZ** and **PTZ-Th** present the thiophene rings more tilted towards the TiO_2 surface than **Calix-PTZ$_2$** (almost 50% of the conformations of **Calix-PTZ** and **PTZ-Th** present angle values $\leq$60°, to be compared with around one quarter for **Calix-PTZ$_2$**).

Regarding the catalyst-dye interaction, Figure 8 depicts the percentage frequency and the cumulative percentage frequency of the distances between the centre of the phenothiazine ring and the ruthenium atom of the catalyst. No significant

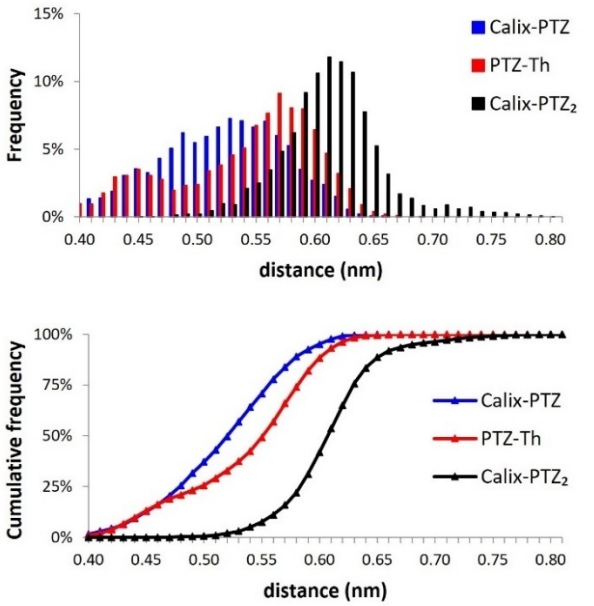

Figure 6. Distances between the center of the thiophene rings and the TiO_2 surface along MD trajectories of **Calix-PTZ/[Ru(bda)(pic)$_2$]**, **Calix-PTZ$_2$/[Ru-(bda)(pic)$_2$]** and **PTZ-Th**: (top) percentage frequency and (bottom) cumulative percentage frequency.

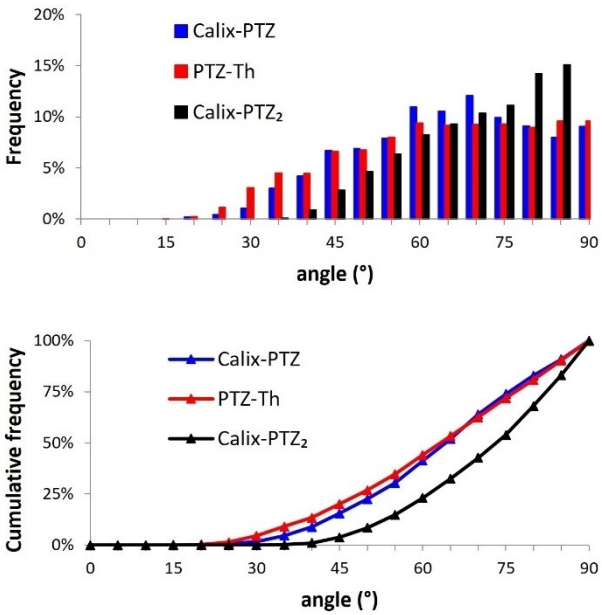

Figure 7. Angles between the thiophene rings and the TiO_2 surface along MD trajectories of **Calix-PTZ/[Ru(bda)(pic)$_2$]**, **Calix-PTZ$_2$/[Ru(bda)(pic)$_2$]** and **PTZ-Th**: (top) percentage frequency and (bottom) cumulative percentage frequency.

differences were observed between the dyads **Calix-PTZ/[Ru-(bda)(pic)$_2$]** and **Calix-PTZ$_2$/[Ru(bda)(pic)$_2$]**.

These results suggest that the higher photocurrent density observed for **Calix-PTZ** with respect to **Calix-PTZ$_2$** could be the result of the different mobility of the dye coordinated to the surface. **Calix-PTZ**, coordinated with two carboxylates to the

Research Article
doi.org/10.1002/ejoc.202200649

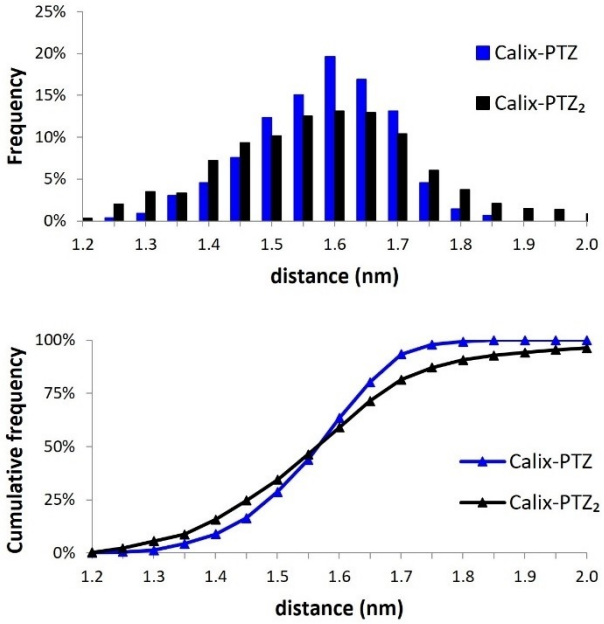

Figure 8. Distances between the centre of the phenothiazine ring and the ruthenium atom of the catalyst along MD trajectories of **Calix-PTZ/[Ru(bda)(pic)$_2$]** and **Calix-PTZ$_2$/[Ru(bda)(pic)$_2$]**: (top) percentage frequency and (bottom) cumulative percentage frequency.

surface, presents greater mobility than **Calix-PTZ$_2$**. Indeed, it adopts conformations that present a presumably more favourable spatial disposition of the dye LUMO involved in the electron injection into the semiconductor.[36] On the contrary, the rigid constraints imposed by the four carboxylates coordination reduce the **Calix-PTZ$_2$** mobility, negatively affecting the possibility to adopt relative orientations favourable to an efficient electron transfer process.

In contrast, no significant differences were observed in the distances involving the ruthenium atom of the catalyst and the HOMO of the dyes, thus indicating that the higher photocurrent density observed for **Calix-PTZ** could mainly be due to the more favourable interaction LUMO-TiO_2.

Finally, comparison between **Calix-PTZ** and **PTZ-Th** shows that these two compounds present similar mobility with respect to the surface. Accordingly, the higher current density observed in **Calix-PTZ** might be attributed to the catalyst proximity to the chromophore which is favoured by the docking of the former into the calix[4]arene cavity.[13]

Conclusion

In this work, we have introduced a novel concept consisting in integrated photosensitizer-catalyst dyads based on host-guest non-covalent interactions through the use of calix[4]arene cavities for solar energy conversion in photoelectrochemical cells. By using such supramolecular approach we were able to achieve enhanced photocurrent photogeneration (twice greater) in the integrated calixarene-based host-guest dyads compared to the conventional arrangement based on two separate photosensitizer and catalyst components. In particular, we have measured that the calix[4]arene derivative carrying only one chromophore unit (**Calix-PTZ**) is much more efficient than the counterpart with two dye units (**Calix-PTZ$_2$**). Molecular dynamics simulations suggest that the superior performance of **Calix-PTZ** could originate from a closer contact of the LUMO of the dye with the surface of the semiconductor compared to **Calix-PTZ$_2$**, thus allowing a more efficient electron transfer from the photoexcited dye to the CB of TiO_2. At the same time, the presence of the calix[4]arene host cavity facilitates a more persistent interaction between the catalyst and the dye, compared to the reference system without the host moiety (**PTZ-Th**).

In conclusion, we believe that these results represent a novel concept for designing efficient integrated supramolecular dye-catalyst components for photoelectrochemical charge generation and subsequent production of solar fuels and chemicals, which can be extended to other families of sensitizers and catalysts for a variety of applications in the field of solar energy conversion and artificial photosynthesis.

Experimental Section

General information

The following materials were purchased from commercial suppliers: FTO-coated glass plates (2.2-mm thick; sheet resistance ~7 ohm per square; Solaronix); Dyesol 18NR–T transparent TiO_2 blend of active 20 nm anatase particles. UV-O_3 treatment was performed using Novascan PSD Pro Series – Digital UV Ozone System. The thickness of the layers was measured by means of a VEECO Dektak 8 Stylus Profiler.

Electrochemical investigation of dyes

Cyclic Voltammetry (CV) was carried out at a scan rate of 50 mV s^{-1}, using a Bio-logic SP-240 potentiostat in a three-electrode electrochemical cell under Ar. The working, counter, and the pseudo-reference electrodes were a glassy carbon pin (surface area = 0.02 cm^2), an Ag/Ag$^+$ TBAP in CH_3CN (0.1 M tetrabutylammonium perchlorate and 0.01 M $AgNO_3$ in acetonitrile) and a Pt wire for the dyes in solution or a sensitized 3.5-μm-thick TiO_2 film, a Pt wire and an Ag/AgCl electrode (3 M KCl) for the measurements on film. The working electrodes discs were well polished with alumina 0.1 μm suspension. The preparation and sensitization of the 3.5-μm-thick TiO_2 film is described below. The Pt wire was sonicated for 15 min in deionized water, washed with 2-propanol, and cycled for 50 times in 0.5 M H_2SO_4 before use. The Ag/Ag$^+$ pseudo-reference electrode was calibrated, by adding ferrocene (10^{-3} M, Fc) to the test solution after each measurement.[37] The Ag/AgCl (KCl 3 M) pseudo-reference electrode was calibrated, by adding potassium hexacyanoferrate(II) trihydrate (10^{-3} M) to the test solution after each measurement.[38] Electrochemistry in solution was performed in $TBABF_4$ 0.1 M DMF, while the one on film in 0.01 M aqueous buffer phosphate saline solution and 0.5 M KNO_3 at pH 6.5. 5% CF_3CH_2OH (v/v) was added to solubilize the WOC in the experiments with the WOC (1×10^{-3} M – final concentration). The potentials were recorded respect to Fc/Fc$^+$ and $[Fe(CN)_6]^{3-}$/$[Fe(CN)_6]^{2-}$ and converted to NHE adding 0.72 V or +0.408 V respectively.[37–38]

Research Article
doi.org/10.1002/ejoc.202200649

Preparation of photoanodes

The photoanodes have been prepared adapting a procedure reported in the literature.[39] In order to exclude metal contamination all the containers were in glass or Teflon and were treated with EtOH and 10% HCl prior to use. Plastic spatulas and tweezers have been used. FTO glass plates were cleaned in a detergent solution for 15 min using an ultrasonic bath, rinsed with pure water and EtOH. After treatment in a UV-O_3 system for 18 min, a transparent active layer of 0.8 cm^2 was screen-printed using Dyesol 18NR-T active transparent TiO_2 paste. The coated films were thermally treated at 125 °C for 6 min, 325 °C for 10 min, 450 °C for 15 min, and 500 °C for 15 min. The heating ramp rate was 5–10 °C min^{-1}.

These films were then treated in a UV-O_3 system for 20 min at room temperature, then soaked into a 2×10^{-4} M solution in EtOH/DMSO (15:1) of the photosensitizer overnight at room temperature in the dark. The stained substrates were rinsed with EtOH and dried with a stream of dry nitrogen. The UV-Vis spectra were recorded in comparison with a bare 1 μm transparent TiO_2 film, while CV and LSV with a bare 3.5 μm transparent TiO_2 film.

Photoelectrochemical measurements

Photoelectrochemical measurements of DS-PEC were carried out with black metal mask on top of the photoanode of 0.50 cm^2 surface area under a 200 W Xenon lamp (using a LOT-Oriel xenon white light source, equipped with a 400 nm cut-off filter to minimize TiO_2 contribution and an IR filter to avoid cell warming). The LSV (scan rate 20 $mV\,s^{-1}$) and CA measurements on the DS-PEC were performed using a Biologic SP-240 potentiostat in a three-electrode purposely designed photoelectrochemical cell filled with pH 6.5 PBS (Sigma Aldrich, product number P4417), KNO_3 0.5 M under Ar, and the data collected with EC-Lab.

Molecular modelling

Starting from the crystallographic structure of anatase [101],[40] a TiO_2 slab (dimensions: 9.2×7.9×1.1 nm) was built with Maestro 2021 suite.[41] The slab was inserted in a simulation box large enough to contain the dyes and the catalyst (final dimensions 9.2×7.9×6.0 nm). The structures of the three dyes and the catalyst were built in Maestro and optimized with *all atom* force field OPLS-2005[42] before approaching them to the surface. The systems were solvated with water molecules described by SPC model (approx. number of water molecules: 12000). Carboxylic groups of the dyes were considered in their anionic form to guarantee the anchoring to the surface. Neutralization of the total charge of the systems was reached by adding Na^+ ions. For titanium dioxide, a force field described only by non-bonded electrostatic and van der Waals interactions was used.[43] This force fields were developed in order to adequately describe both the bulk and the water surface interactions of TiO_2. The all-atom force field OPLS-2005 was used for the photosensitizers and the catalyst.[42] Molecular Dynamics simulations were performed with Gromacs (release 2019.1),[44] applying Periodic Boundary Conditions. For non-bonded interactions a 1.2 nm cut-off was used, beyond which long-range electrostatic interactions were treated by Particle Mesh Ewald algorithm.[45] Systems were minimized with steepest descent algorithm. Initial velocities were generated from a Maxwell distribution at 300 K with a random seed. MD simulations were performed at constant temperature (T = 300 K) and pressure (P = 1 bar) with a 2 fs time-step. TiO_2 surface, dyes, catalyst and aqueous solutions were coupled to V-rescale thermostats[46] every 0.1 ps and to a Parrinello-Rahman barostat[47] every 2 ps. Bonds involving hydrogen atoms were constrained with LINCS algorithm.[48] For each system two 50 ns simulations were run and analysed every 100 ps.

As far as quantomechanical calculations are concerned, we considered a model of the **PTZ** dye (Figure S6), where the alkyl chain of **PTZ-Th** has been replaced by a methyl group. Ground state geometry optimization of this model dye was performed by a density functional theory (DFT) calculation in vacuo, with PBE0 functional[49] and 6-31G* basis set by using the Gaussian 16 program (revision A.03).[50] The calculated HOMO and LUMO at the PBE0/6-31G* level are shown in Figure S7.

General information for synthesis

NMR spectra were recorded with a Bruker Advance-Neo spectrometer operating at 400 MHz (^{1}H) and 100 MHz (^{13}C). Coupling constants are given in Hz. Absorption spectra were recorded with a V-570 Jasco spectrophotometer. ATR FT-IR spectra were recorded with a PerkinElmer Spectrum 100. High resolution mass spectra have been recorded with an Agilent 6230B Time of Flight (TOF) equipped with an electrospray (dual ESI) source. Compounds were purified using flash chromatography with Merck grade 9385 silica gel 230–400 mesh (60 Å). The glassware for water-free reactions was dried in a 130 °C oven for 4 h before use and then attached to the vacuum pump. Inert atmosphere was generated by Schlenk technique using nitrogen flow. Conversion was monitored by thin-layer chromatography (Silica gel on TLC Al foils with fluorescent indicator 254 nm) by using UV light (254 and 365 nm) as a visualizing agent. All reagents were obtained from commercial suppliers at the highest purity grade and used without further purification. Anhydrous solvents were purchased from Acros Organics and used without further purification. Organic phases obtained after extraction were dried with Na_2SO_4 and filtered before removal of the solvent by evaporation. The **PTZ-Th**,[25a] 4,4,5,5-tetramethyl-2-(5-(4,4,5,5-tetramethyl-1,3-dioxolan-2-yl)thiophen-2-yl)-1,3,2-dioxaborolane,[27] 5,11,17,23-tetra-tert-butyl-25,26,27-tripropoxycalix[4]arene (**1**),[26] 5,11,17,23-tetra-*tert*-butyl-25,27-dipropoxycalix[4]arene (**3**),[26] and **[Ru(bda)(pic)$_2$]**,[24a] have been synthesized according to literature procedures. The synthetic procedures for all the new synthesized compounds are described in the Supporting Information.

Acknowledgements

Prof. Ivano Eberini (University of Milan) is gratefully acknowledged for providing the access to the Maestro Suite 2021–3 (Schrödinger Inc.) for the setup of the systems to be submitted to MD simulations. The computations were carried out on high-performance computing resources provided by CINECA as part of the agreement with the University of Milano-Bicocca. This work was carried out under the framework of the national PRIN project "Unlocking Sustainable Technologies Through Nature-inspired Solvents" (NATUREChem) (grant number: 2017 A5HXFC 002). The authors wish to acknowledge the Ministero dell'Università e della Ricerca (MUR) for this financial support. Financial support from MUR (grant Dipartimenti di Eccellenza – 2017 "Materials for Energy") and University of Milano-Bicocca (Fondo di Ateneo – Quota Competitiva 2017 and 2019, Bando Infrastrutture di Ricerca 2021) is also gratefully acknowledged by C. L. B., C. D., N. M., and A. A. F. F., F. S and L. B. wish to acknowledge the Italian Ministry of Instruction, University and Research (COMP-HUB initiative,

Departments of Excellence Program) for financial support. Open Access funding provided by Università degli Studi di Milano-Bicocca within the CRUI-CARE Agreement.

Conflict of Interest

The authors declare no conflict of interest.

Data Availability Statement

The data that support the findings of this study are available from the corresponding author upon reasonable request.

Keywords: Water splitting · Photoelectrochemistry · Dye-sensitized · Molecular dynamics · Calix[4]arene

[1] G. Pleßmann, P. Blechinger, *Energy Strategy Rev.* **2017**, *15*, 19–32.
[2] a) J. Chow, R. J. Kopp, P. R. Portney, *Science* **2003**, *302*, 1528–1531; b) N. Armaroli, V. Balzani, *Chem. Asian J.* **2011**, *6*, 768–784; c) N. Armaroli, V. Balzani, *Energy Environ. Sci.* **2011**, *4*, 3193; d) N. Armaroli, V. Balzani, *ChemSusChem* **2011**, *4*, 21–36.
[3] P. G. Levi, J. M. Cullen, *Environ. Sci. Technol.* **2018**, *52*, 1725–1734.
[4] a) J. H. Kim, D. Hansora, P. Sharma, J.-W. Jang, J. S. Lee, *Chem. Soc. Rev.* **2019**, *48*, 1908–1971; b) K. Chandrasekhar, S. Kumar, B.-D. Lee, S.-H. Kim, *Bioresour. Technol.* **2020**, *302*, 122920; c) M. Kamaraj, K. K. Ramachandran, J. Aravind, *IJEST* **2020**, *17*, 559–576; d) S. Li, Q. Kang, J. Baeyens, H. L. Zhang, Y. M. Deng, *IOP Conf. Ser.: Earth Environ. Sci.* **2020**, *544*, 012011; e) S. Atilhan, S. Park, M. M. El-Halwagi, M. Atilhan, M. Moore, R. B. Nielsen, *Curr. Opin. Chem. Eng.* **2021**, *31*, 100668; f) K. Espegren, S. Damman, P. Pisciella, I. Graabak, A. Tomasgard, *Int. J. Hydrogen Energy* **2021**, *46*, 23125–23138; g) K. Hainsch, K. Löffler, T. Burandt, H. Auer, P. Crespo del Granado, P. Pisciella, S. Zwickl-Bernhard, *Energy* **2022**, *239*, 122067; h) T. Faunce, *Procedia Eng.* **2012**, *49*, 348–356; i) N. Armaroli, V. Balzani, *Chem. Eur. J.* **2016**, *22*, 32–57.
[5] a) M. Watanabe, *Sci. Technol. Adv. Mater.* **2017**, *18*, 705–723; b) P. Xu, N. S. McCool, T. E. Mallouk, *Nano Today* **2017**, *14*, 42–58; c) C. Decavoli, C. L. Boldrini, N. Manfredi, A. Abbotto, *Rend. Lincei Sci. Fis. Nat.* **2019**, *30*, 469–483; d) S. Yun, N. Vlachopoulos, A. Qurashi, S. Ahmad, A. Hagfeldt, *Chem. Soc. Rev.* **2019**, *48*, 3705–3722; e) C. Decavoli, C. L. Boldrini, N. Manfredi, A. Abbotto, *Eur. J. Inorg. Chem.* **2020**, *2020*, 978–999; f) K. Hu, R. N. Sampaio, J. Schneider, L. Troian-Gautier, G. J. Meyer, *J. Am. Chem. Soc.* **2020**, 10.1021/jacs.0c04886; g) B. D. Sherman, N. K. McMillan, D. Willinger, G. Leem, *Nano Convergence* **2021**, *8*, 7; h) M. K. Brennaman, R. J. Dillon, L. Alibabaei, M. K. Gish, C. J. Dares, D. L. Ashford, R. L. House, G. J. Meyer, J. M. Papanikolas, T. J. Meyer, *J. Am. Chem. Soc.* **2016**, *138*, 13085–13102.
[6] B. Cecconi, N. Manfredi, T. Montini, P. Fornasiero, A. Abbotto, *Eur. J. Org. Chem.* **2016**, *2016*, 5194–5215.
[7] M. Grätzel, *Nature* **2001**, *414*, 338.
[8] W. J. Youngblood, S.-H. A. Lee, K. Maeda, T. E. Mallouk, *Acc. Chem. Res.* **2009**, *42*, 1966–1973.
[9] a) N. Manfredi, B. Cecconi, A. Abbotto, *Eur. J. Org. Chem.* **2014**, *2014*, 7069–7086; b) A. Mahmood, *Sol. Energy* **2016**, *123*, 127–144; c) G. Richhariya, A. Kumar, P. Tekasakul, B. Gupta, *Renewable Sustainable Energy Rev.* **2017**, *69*, 705–718; d) S. Alhorani, S. Kumar, M. Genwa, P. L. Meena, *AIP Conf. Proc.* **2020**, *2265*, 030632; e) D. Devadiga, M. Selvakumar, P. Shetty, M. S. Santosh, *J. Power Sources* **2021**, *493*, 229698.
[10] a) J. F. Huang, Y. Lei, T. Luo, J. M. Liu, *ChemSusChem* **2020**, *13*, 5863–5895; b) J. Warnan, E. Reisner, *Angew. Chem. Int. Ed.* **2020**, *59*, 17344–17354; *Angew. Chem.* **2020**, *132*, 17496–17506; c) S. Zhang, H. Ye, J. Hua, H. Tian, *EnergyChem* **2019**, *1*, 100015; d) M.-N. Collomb, D. V. Morales, C. N. Astudillo, B. Dautreppe, J. Fortage, *Sustain. Energy Fuels* **2020**, *4*, 31–49; e) N. Vlachopoulos, A. Hagfeldt, *Chimia* **2019**, *73*, 894; f) F. Niu, D. Wang, F. Li, Y. Liu, S. Shen, T. J. Meyer, *Adv. Energy Mater.* **2020**, *10*, 1900399.
[11] a) M. V. Sheridan, B. D. Sherman, R. L. Coppo, D. Wang, S. L. Marquard, K.-R. Wee, N. Y. Murakami Iha, T. J. Meyer, *ACS Energy Lett.* **2016**, *1*, 231–236; b) Y. Zhu, D. Wang, Q. Huang, J. Du, L. Sun, F. Li, T. J. Meyer, *Nat. Commun.* **2020**, *11*, 4610; c) I. Grądzka-Kurzaj, M. Gierszewski, B. J. J. Timmer, M. Ziółek, *ACS Appl. Mater. Interfaces* **2021**, *4*, 2440–2450.
[12] a) D. Anton-Garcia, J. Warnan, E. Reisner, *Chem. Sci.* **2020**, *11*, 12769–12776; b) M. Yamamoto, L. Wang, F. Li, T. Fukushima, K. Tanaka, L. Sun, H. Imahori, *Chem. Sci.* **2016**, *7*, 1430–1439; c) C. Decavoli, C. L. Boldrini, V. Trifiletti, S. Luong, O. Fenwick, N. Manfredi, A. Abbotto, *RSC Adv.* **2021**, *11*, 5311–5319; d) N. Kaeffer, J. Massin, C. Lebrun, O. Renault, M. Chavarot-Kerlidou, V. Artero, *J. Am. Chem. Soc.* **2016**, *138*, 12308–12311; e) B. D. Sherman, Y. Xie, M. V. Sheridan, D. Wang, D. W. Shaffer, T. J. Meyer, J. J. Concepcion, *ACS Energy Lett.* **2017**, *2*, 124–128.
[13] H. Li, F. Li, Y. Wang, L. Bai, F. Yu, L. Sun, *ChemPlusChem* **2016**, *81*, 1056–1059.
[14] a) A. Casnati, *Chem. Commun.* **2013**, *49*, 6827–6830; b) S. E. Matthews, P. D. Beer, *Supramol. Chem.* **2005**, *17*, 411–435; c) F. Sansone, L. Baldini, A. Casnati, R. Ungaro, *New J. Chem.* **2010**, *34*, 2715–2728.
[15] a) G. Pognon, J. A. Wytko, P. D. Harvey, J. Weiss, *Chem. Eur. J.* **2009**, *15*, 524–535; b) I. Tosi, M. Segado Centellas, E. Campioli, A. Iagatti, A. Lapini, C. Sissa, L. Baldini, C. Cappelli, M. Di Donato, F. Sansone, F. Santoro, F. Terenziani, *ChemPhysChem* **2016**, *17*, 1686–1706.
[16] a) K. Helttunen, P. Shahgaldian, *New J. Chem.* **2010**, *34*, 2704–2714; b) S. Pasquale, S. Sattin, E. C. Escudero-Adán, M. Martínez-Belmonte, J. de Mendoza, *Nat. Commun.* **2012**, *3*, 785; c) R. Kumar, A. Sharma, H. Singh, P. Suating, H. S. Kim, K. Sunwoo, I. Shim, B. C. Gibb, J. S. Kim, *Chem. Rev.* **2019**, *119*, 9657–9721.
[17] a) A. Arduini, F. F. Nachtigall, A. Pochini, A. Secchi, F. Ugozzoli, *Supramol. Chem.* **2000**, *12*, 273–291; b) G. Arena, A. Contino, A. Magrì, D. Sciotto, A. Arduini, A. Pochini, A. Secchi, *Supramol. Chem.* **2001**, *13*, 379–386; c) H. Li, F. Qu, *J. Mater. Chem.* **2007**, *17*, 3536–3544.
[18] a) Y. Liu, E.-C. Yang, Y. Chen, D.-S. Guo, F. Ding, *Eur. J. Org. Chem.* **2005**, *2005*, 4581–4588; b) C. Bonaccorso, C. Sgarlata, G. Grasso, V. Zito, D. Sciotto, G. Arena, *Chem. Commun.* **2011**, *47*, 6117–6119.
[19] C. L. Boldrini, N. Manfredi, T. Montini, L. Baldini, A. Abbotto, P. Fornasiero, *Curr. Opin. Green Sustain. Chem.* **2021**, *32*, 100534.
[20] C. Decavoli, PhD Thesis, University of Milano-Bicocca, 2022. DOI: http://hdl.handle.net/10281/376409.
[21] G. D. Andreetti, R. Ungaro, A. Pochini, *J. Chem. Soc. Chem. Commun.* **1979**, 10.1039/C39790001005, 1005–1007.
[22] J. M. Notestein, A. Katz, E. Iglesia, *Langmuir* **2006**, *22*, 4004–4014.
[23] A. Arduini, R. Caciuffo, S. Geremia, C. Ferrero, F. Ugozzoli, F. Zontone, *Supramol. Chem.* **1998**, *10*, 125–132.
[24] a) L. Duan, A. Fischer, Y. Xu, L. Sun, *J. Am. Chem. Soc.* **2009**, *131*, 10397–10399; b) L. Li, L. Duan, Y. Xu, M. Gorlov, A. Hagfeldt, L. Sun, *Chem. Commun.* **2010**, *46*, 7307–7309.
[25] a) B. Cecconi, N. Manfredi, R. Ruffo, T. Montini, I. Romero-Ocana, P. Fornasiero, A. Abbotto, *ChemSusChem* **2015**, *8*, 4216–4228; b) N. Manfredi, B. Cecconi, V. Calabrese, A. Minotti, F. Peri, R. Ruffo, M. Monai, I. Romero-Ocana, T. Montini, P. Fornasiero, A. Abbotto, *Chem. Commun.* **2016**, *52*, 6977–6980; c) N. Manfredi, M. Monai, T. Montini, M. Salamone, R. Ruffo, P. Fornasiero, A. Abbotto, *Sustain. Energy Fuels* **2017**, *1*, 694–698.
[26] K. Iwamoto, K. Araki, S. Shinkai, *J. Org. Chem.* **1991**, *56*, 4955–4962.
[27] V. Leandri, R. Ruffo, V. Trifiletti, A. Abbotto, *Eur. J. Org. Chem.* **2013**, *2013*, 6793–6801.
[28] M. Castillo-Valles, J. M. Andres-Castan, J. Garin, J. Orduna, B. Villacampa, S. Franco, M. J. Blesa, *RSC Adv.* **2015**, *5*, 90667–90670.
[29] J. Tauc, *Mater. Res. Bull.* **1968**, *3*, 37–46.
[30] H. Tian, G. Boschloo, A. Hagfeldt *Molecular Devices for Solar Energy Conversion and Storage*, Springer, Singapore, **2018**.
[31] J. O. M. Bockris, A. K. N. Reddy, M. E. Gamboa-Aldeco, *Modern Electrochemistry 2 A: Fundamentals of Electrodics*, Springer, Boston, MA, **2000**.
[32] F. Li, K. Fan, L. Wang, Q. Daniel, L. Duan, L. Sun, *ACS Catal.* **2015**, *5*, 3786–3790.
[33] J. T. Kirner, J. J. Stracke, B. A. Gregg, R. G. Finke, *ACS Appl. Mater. Interfaces* **2014**, *6*, 13367–13377.
[34] a) D. H. Brouwer, S. Alavi, J. A. Ripmeester, *Phys. Chem. Chem. Phys.* **2008**, *10*, 3857–3860; b) E. B. Brouwer, G. D. Enright, J. A. Ripmeester, *Supramol. Chem.* **1996**, *7*, 143–145.
[35] B. Lemli, J. Peles, L. Kollár, G. Nagy, S. Kunsági-Máté, *Supramol. Chem.* **2006**, *18*, 251–256.
[36] D. L. Ashford, W. Song, J. J. Concepcion, C. R. K. Glasson, M. K. Brennaman, M. R. Norris, Z. Fang, J. L. Templeton, T. J. Meyer, *J. Am. Chem. Soc.* **2012**, *134*, 19189–19198.

[37] D. T. Sawyer, A. Sobkowiak, J. L. Roberts, *Electrochemistry for Chemists*, 2nd ed., Wiley, New York, USA, **1995**.
[38] J. E. O'Reilly, *Biochim. Biophys. Acta Bioenerg.* **1973**, *292*, 509–515.
[39] S. Ito, T. N. Murakami, P. Comte, P. Liska, C. Grätzel, M. K. Nazeeruddin, M. Grätzel, *Thin Solid Films* **2008**, *516*, 4613–4619.
[40] C. J. Howard, T. M. Sabine, F. Dickson, *Acta Crystallogr.* **1991**, *47*, 462–468.
[41] Schrödinger Release 2021–3: Maestro, Schrödinger, LLC, New York, NY, 2021.
[42] J. L. Banks, H. S. Beard, Y. Cao, A. E. Cho, W. Damm, R. Farid, A. K. Felts, T. A. Halgren, D. T. Mainz, J. R. Maple, R. Murphy, D. M. Philipp, M. P. Repasky, L. Y. Zhang, B. J. Berne, R. A. Friesner, E. Gallicchio, R. M. Levy, *J. Comput. Chem.* **2005**, *26*, 1752–1780.
[43] E. G. Brandt, A. P. Lyubartsev, *J. Phys. Chem. C* **2015**, *119*, 18110–18125.
[44] M. J. Abraham, T. Murtola, R. Schulz, S. Páll, J. C. Smith, B. Hess, E. Lindahl, *SoftwareX* **2015**, *1–2*, 19–25.
[45] T. Darden, D. York, L. Pedersen, *J. Chem. Phys.* **1993**, *98*, 10089–10092.
[46] G. Bussi, D. Donadio, M. Parrinello, *J. Chem. Phys.* **2007**, *126*, 014101.
[47] M. Parrinello, A. Rahman, *J. Appl. Phys.* **1981**, *52*, 7182–7190.
[48] B. Hess, H. Bekker, H. J. C. Berendsen, J. G. E. M. Fraaije, *J. Comput. Chem.* **1997**, *18*, 1463–1472.
[49] C. Adamo, V. Barone, *J. Chem. Phys.* **1999**, *110*, 6158–6170.
[50] Gaussian 16 Rev. A.03 (Wallingford, CT, 2016).

Manuscript received: June 1, 2022
Revised manuscript received: July 22, 2022